1999 Turbomachinery Committee Best Paper Award

Development of Advanced Compressor Airfoils for Heavy-Duty Gas Turbines—Part II: Experimental and Theoretical Analysis

Bernhard Küsters[1]
Heinz-Adolf Schreiber

German Aerospace Center,
Institute of Propulsion Technology,
D-51170 Köln, Germany

Ulf Köller
Reinhard Mönig

Siemens AG,
Power Generation (KWU),
D-45466 Mülheim a.d. Ruhr, Germany

In Part I of this paper a family of numerically optimized subsonic compressor airfoils for heavy-duty gas turbines, covering a wide range of flow properties, is presented. The objective of the optimization was to create profiles with a wide low loss incidence range. Therefore, design point and off-design performance had to be considered in an objective function. The special flow conditions in large-scale gas turbines have been taken into account by performing the numerical optimization procedure at high Reynolds numbers and high turbulence levels. The objective of Part II is to examine some of the characteristics describing the new airfoils, as well as to prove the reliability of the design process and the flow solver applied. Therefore, some characteristic members of the new airfoil series have been extensively investigated in the cascade wind tunnel of DLR cologne. Experimental and numerical results show profile Mach number distributions, total pressure losses, flow turning, and static pressure rise for the entire incidence range. The design goal with low losses and especially a wide operating range could be confirmed, as well as a mild stall behavior. Boundary layer development, particularly near stall condition, is discussed using surface flow visualization and the results of boundary layer calculations. An additional experimental study, using liquid crystal coating, provides necessary information on suction surface boundary-layer transition at high Reynolds numbers. Finally, results of Navier–Stokes simulations are presented that enlighten the total pressure loss development and flow turning behavior, especially at high incidence in relation to the results of the design tool. [S0889-504X(00)02602-7]

Introduction

Efficiency improvements of axial flow compressors are directly linked to the aerodynamic quality and the performance characteristic of the blade elements. Also stable operating conditions at off-design depend on boundary layer separation behavior and flow turning characteristics of the cascades. Furthermore, a wide low-loss incidence range of the profiles allows some uncertainty in predicting the design point during the preliminary design without significant penalty in efficiency and enables a large stall margin.

In the past, a variety of numerical blade-to-blade methods have been successfully applied for tailoring the blade profiles. Thereby either direct or inverse methods were applied, both to analyze or define blade contours that satisfy the vector diagrams set by the preliminary throughflow design. Both inverse and direct methods basically have already been used as automated design tools and had been embedded in special numerical optimization algorithms which search, for example, for maximum efficiency at the design point or maximum loading.

Substantial improvements apart from the pure design point optimization, however, can be achieved only by employment of direct solvers, by which off-design performance can be analyzed and considered in the optimization process. Thereby, special aerodynamic features of the cascade, such as flow turning, minimum loss, or special boundary layer behavior at off-design, can be asked for. This, however, involves considerable time-consuming blade-to-blade calculations and corresponding high computer performance. Using a fast and robust flow solver, the optimization process can nowadays be performed in a reasonable and acceptable time.

In Part I of this paper [1], the development of such an automated design system is described. This tool was then used to tailor a new family of subsonic airfoils suitable for heavy-duty gas turbine compressors. Design and optimization considered the specific boundary conditions of these large compressors, taking into account the effect of the high Reynolds number on boundary layer development and transition. The profile optimization process minimized an objective function that aimed for a low loss level in the entire operating range, a wide incidence range, and a certain stall margin. The blade-to-blade code used in this optimization process was the Q3D Euler solver MISES from Drela and Youngren [2–4] in its direct mode. It is a coupled inviscid/viscous interaction method that employs integral boundary layer equations for boundary layer and wake development. Boundary layer transition is predicted with the modified criterion of Abu-Ghannam/Shaw [5,6].

The objective of the present work was to validate the design process and to check whether the design goals like flow turning, loss level, incidence range, and stall margin were achieved. This involved the validation of the blade-to-blade solver, especially at off-design operating points.

For this reason four typical airfoil sections of the new family

[1]Now with Siemens AG.

Contributed by the International Gas Turbine Institute and presented at the 44th International Gas Turbine and Aeroengine Congress and Exhibition, Indianapolis, Indiana, June 7–10, 1999. Manuscript received by the International Gas Turbine Institute February 1999. Paper No. 99-GT-96. Review Chair: D. C. Wisler.

have been tested in a wide range of inlet Mach numbers, inlet flow angles and at different AVDR values. Again, the blade-to-blade solver MISES was used to elucidate the boundary layer behavior and special features of the aerodynamic characteristics. Additionally, a modern Navier–Stokes solver has been applied to one of the cascades to give further information, especially on differences between experiment and MISES calculation.

Further emphasis was placed on a critical assessment of the boundary layer transition model, implemented in the MISES code. Therefore, an additional experiment was conducted to determine the impact of Reynolds number and turbulence level on the transition process. A validation of the transition model was of specific interest because at high Reynolds numbers and high turbulence levels, transition onset moved to the front portion of the blades. This had an essential impact on the optimized blade pressure distribution and the corresponding profile geometry.

Description of the Cascades

Design considerations for the optimized cascades focused on high aerodynamic efficiency and a stable wide operating range. In contrast to aeroengine compressors, an increase of blade loading and a drastic reduction of the number of blade rows is less important for an industrial large gas turbine.

Therefore, the Mach number level, flow turning, and gap-chord ratios of the developed profile family are moderate at the design point. For sample validation of the new profile family, four different cascades have been selected. These cascades are typical candidates for rotor or stator blade sections of the subsonic part of a multistage compressor [7].

After specifying the aerodynamic requirements for each cascade, such as inlet Mach number, inlet flow angle, flow turning, the AVDR, and gap-chord ratio as well as blade thickness, the geometry parameters prescribing the single blade shape are derived using the correlations of the complete profile systematic [8].

The design parameters of the four representative cascades are listed in Table 1, and Fig. 1 shows the corresponding geometry. Due to a moderate aerodynamic loading, with flow turning between 10 and 18 deg and gap/chord ratios from 0.89 to 0.95, the diffusion factors show values between 0.39 to 0.42.

As already described in Part I of this paper, the blades have been designed and optimized at a Reynolds number of 2.5×10^6, which corresponds to the average Reynolds number of the blade elements in the real large gas turbine compressor [8]. Furthermore, the turbulence level was set to a relatively high value at which laminar-turbulent boundary layer transition on the blade surface occurs mostly in the so-called bypass mode [9]. Under the conditions of high turbulence level and high Reynolds number, transition starts at about 4–8 percent of chord on the blade suction side and 3–4 percent of chord on the pressure side. Transition onset on the suction side is relatively insensitive to the flow acceleration rate.

Table 1 Design parameters of the test cascades

Cascade	A	B	C	D
M_1	0.715	0.607	0.556	0.438
β_1	149.4°	142.0°	147.3°	137.0°
$\Delta\beta$	10.3°	14.7°	12.8°	18.0°
AVDR	1.06	1.05	1.05	0.99
s/c	0.885	0.888	0.953	0.874
DF	0.393	0.393	0.407	0.422
t/c	5.0%	7.0%	7.4%	9.3%

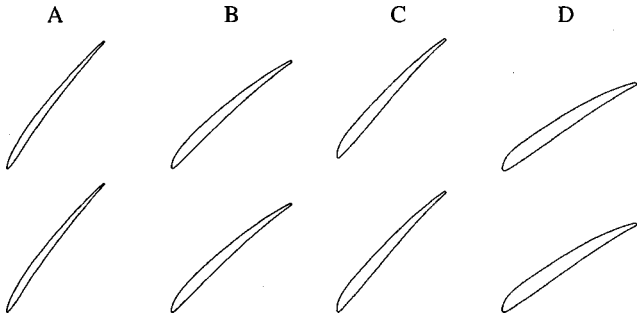

Fig. 1 Test cascades

Consequently, the blade design optimization finished with a forward loaded pressure distribution with a suction surface peak velocity near 8–12 percent of chord. This high peak, where the boundary layer is already turbulent, is immediately followed by a relatively high diffusion rate, which becomes progressively less severe farther downstream. Due to the forward-loaded pressure distribution typical for the whole profile family, all blades have a relatively thick front portion and a low overall camber. Also, the blade stagger angles are considerably lower than stagger angles of corresponding CDA blades with more camber in the rear.

Cascade *A* with an inlet Mach number of 0.715, a flow turning of 10.3 deg, and 5 percent maximum blade thickness was selected to be a typical candidate for a rotor section in one of the forward compressor stages. Furthermore, due to its relatively high inlet Mach number, it was of interest to validate the blade-to-blade code for supercritical flow conditions which are achieved at high positive and negative incidence angles. To limit surface Mach numbers that exceed sonic velocities, the optimization process flattened the velocity peak of blade *A* in the front portion. The corresponding design Mach number distribution of this cascade is plotted in Fig. 2, left.

The character of the profile velocity distribution of the cascades *B*, *C*, and *D* (Fig. 2), which are designed for lower inlet Mach

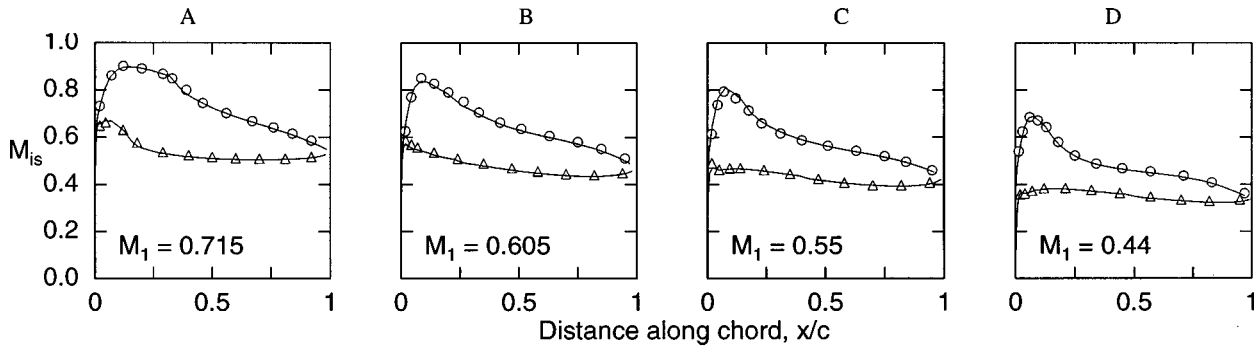

Fig. 2 Experimental and numerical design Mach number distributions of the four test cascades

Table 2 Experimental and MISES data of the four test cascades at design conditions with Re=0.9–0.7×10^6

Cascade	A		B		C		D	
	Experiment	MISES	Experiment	MISES	Experiment	MISES	Experiment	MISES
M_1	0.715	0.715	0.606	0.607	0.555	0.556	0.441	0.440
β_1	149.5°	149.5°	142.0°	142.0°	147.3°	147.3°	137.0°	137.0°
β_2	139.1°	139.2°	127.7°	127.3°	134.4°	134.6°	119.7°	119.3°
AVDR	1.06	1.06	1.05	1.05	1.05	1.05	1.00	0.99
ω	0.0175	0.0161	0.0153	0.0152	0.0164	0.0152	0.0179	0.0155

numbers 0.6, 0.55, and 0.44, is more or less identical, although flow turning and profile thickness differ considerably (see Tables 1 and 2). It is worth mentioning that cascade *D*, with a blade thickness of 9.3 percent of chord and an inlet Mach number of 0.44, was optimized for an incidence angle range of 27 degrees. It could serve, for example, as a rotor hub section in one of the rear stages.

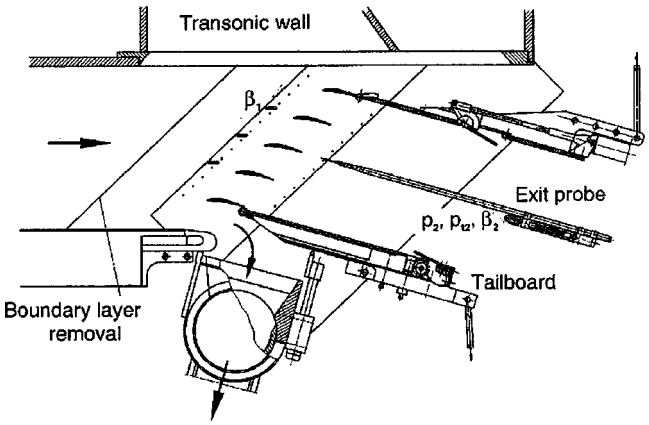

Fig. 3 Cross section of the DLR Transonic Cascade Tunnel

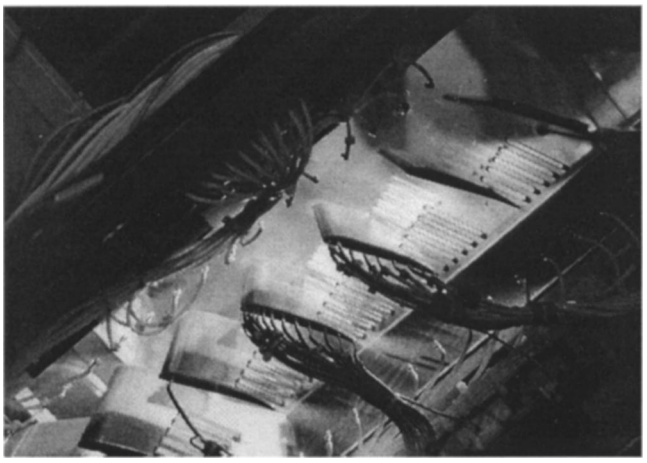

Fig. 4 Photograph of the test section

Table 3 Estimated uncertainties

Upstream flow angle, β_1	± 0.2 - 0.4 deg.
Exit flow angle, β_2	± 0.2 -0.4 deg.
Loss coefficient, ω	± 0.0008
AVDR	± 0.01

Test Procedure

The four optimized cascades were extensively tested in the Transonic Cascade Tunnel of the DLR in Cologne. This tunnel is a closed loop, continuously running facility with a variable nozzle, an upper transonic wall, and a variable test section height. The air supply system enables an inlet Mach number range from 0.2 to 1.4 and a Mach number independent variation of the Reynolds number from about 1×10^5 to 3×10^6. Tunnel sidewall boundary layers ahead of the cascade are removed through protruding slots. Tailboards combined with throttles are used to control inlet and exit boundary conditions and periodicity. Endwall boundary layers and the axial velocity density ratio, AVDR, are controlled using a suction system with suction slots located within the blade pack aft of the minimum pressure region (see Fig. 4).

A cross section and a photograph of the test section are shown in Figs. 3 and 4. For the present tests, 6 blades with 70 mm chord and an aspect ratio of 2.4 are installed. Tests were run with a total pressure of about 1.1 bar and a total temperature of 305 K, giving a Reynolds number of 0.7 to 1.1×10^6 for the investigated Mach number range from about 0.4 to 0.85.

The inlet flow angle is measured with probes at the same gapwise locations for three consecutive blade channels. Furthermore, three center blades have been instrumented on the suction side to control flow periodicity and allow an additional flow angle determination [10,11]. The test procedure is to vary Mach number at each inlet angle for three different AVDR values. Prior to the tests, each individual test point has been precalculated using the blade-to-blade code MISES V2.4. The theoretical profile Mach number distribution, displayed real time together with the test data, served as a goal for the experimental distribution while adjusting the test conditions. By so doing, measurement accuracy, especially of the inlet flow angle and AVDR could be improved considerably. Table 3 provides some estimated uncertainties for key dependent variables, in which uncertainty is less near the design flow conditions and increases approaching the stalled flow conditions.

Test and Design Conditions

Before starting the entire test program, numerical blade-to-blade calculations have been performed to prove the usability of the experimental results for the assessment of the design. Especially, it was of interest to know whether the design flow turning, pressure ratio, and design incidence range, which have been calculated for the high Reynolds number and turbulence level, could be expected also from the experiments in the cascade wind tunnel.

All calculations for design and optimization were performed at a Reynolds number of 2.5×10^6 and a turbulence level of 3 percent, whereas the wind tunnel tests operated at a Reynolds number of $0.7-1.1\times10^6$ and a turbulence level between 0.5 and 1.0 percent. For cascade *C*, which has been designed for an inlet Mach number of 0.55 and a flow turning of 12.8 deg, blade performance was calculated in the entire operating range from negative to positive stall at both design and test conditions. Results in Fig. 5 show that the calculated total pressure losses have the same level and that the inlet flow angle range is practically identical. For all in-

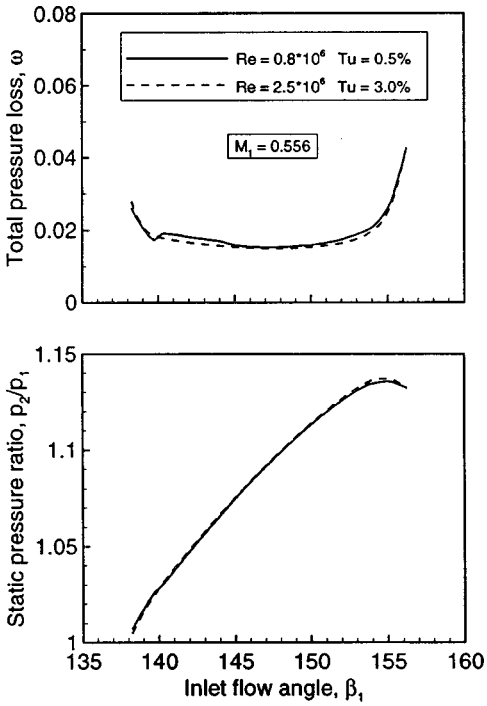

Fig. 5 Predicted performance at different Reynolds numbers, cascade *C*

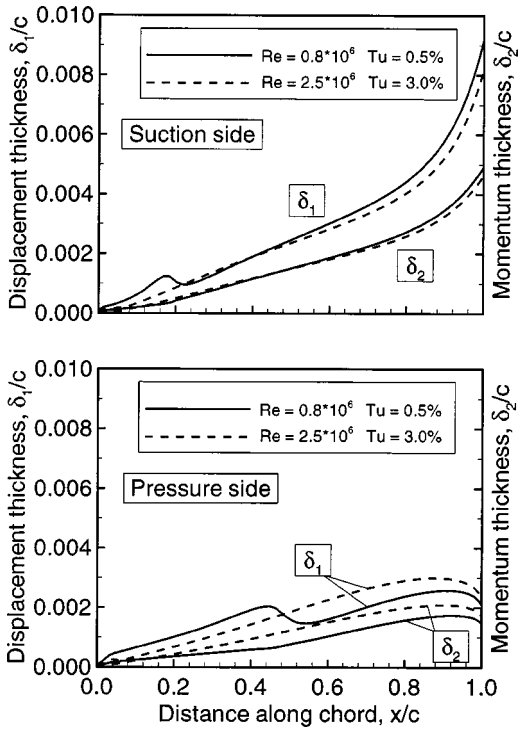

Fig. 7 Boundary layer thickness at different Reynolds numbers, cascade *C*, $M_1=0.556$, $\beta_1=147.3$ deg

cidences and especially at design condition ($\beta_1=147.3$ deg), the profile Mach number distributions shown in Fig. 6 are nearly identical.

Also, the static pressure ratio, which directly depends on flow turning and total pressure loss, is identical in the whole operating range. Marginally higher total pressure losses are normal for low Reynolds numbers, because at low Reynolds numbers boundary layers are slightly thicker. Furthermore, at negative incidences the pressure side shows a short laminar separation behind the leading edge, and at positive incidences the suction side has a small laminar bubble between 14–20 percent of chord. Both effects induce a further marginal increase in total pressure loss. Due to the different boundary layer transition behavior at low and high Reynolds numbers, the boundary layer development on the blade front portion is considerably different. However, for the overall blade performance and the boundary layer thickness at the blade trailing edge, this is of minor influence. The corresponding development of the displacement thickness δ_1, and momentum thickness δ_2, as well as the boundary layer form factor is shown in Figs. 7 and 8 for design and test conditions.

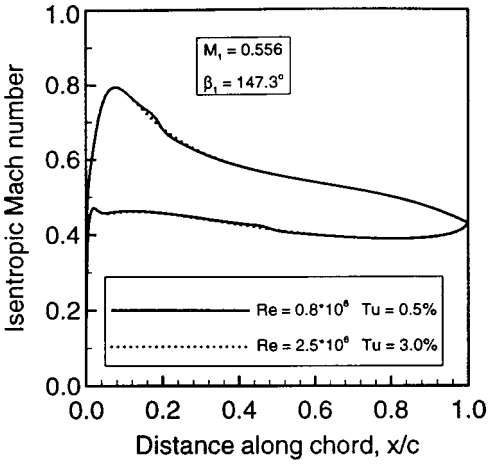

Fig. 6 Isentropic Mach number distribution at different Reynolds numbers, cascade *C*

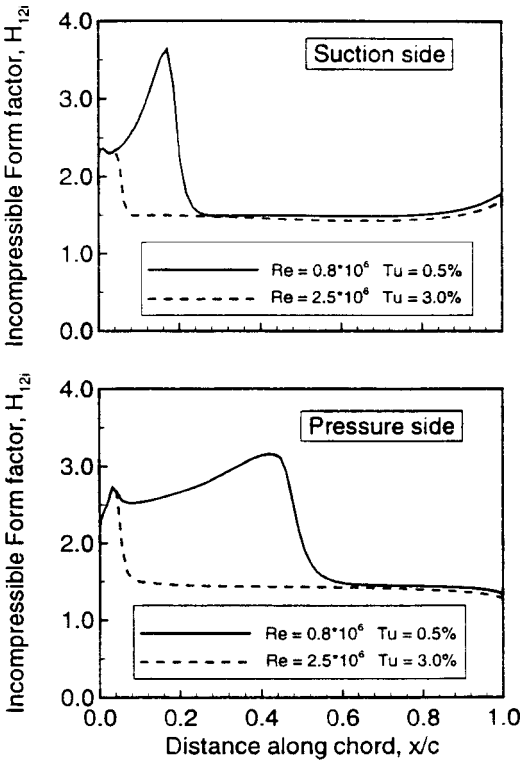

Fig. 8 Boundary layer form factor at different Reynolds numbers, cascade *C*, $M_1=0.556$, $\beta_1=147.3$ deg

Due to the forward-loaded pressure distribution, transition on the blade suction side occurs relatively early, either due to bypass transition at 7 percent of chord or in a laminar separation bubble at 18 percent of chord. Therefore, the essential decelerating part of the suction surface is turbulent and boundary layer thickness as well as the form factors achieve nearly identical values at the trailing edge. Furthermore, even the slightly thicker boundary layer on the suction side for the lower Reynolds number, is compensated by a somewhat smaller boundary layer thickness on the pressure side.

Validation of Design

The test program for each individual cascade covered the complete precalculated incidence range and a certain Mach number variation around design.

An excellent agreement between experiment and numerical analysis using MISES was achieved at the design point for all four cascades. The experimental profile Mach number distributions exactly fit the calculations (Fig. 2), and even exit flow angles agree within the experimental accuracy. A comparison of the design point data is given in Table 2 for wind tunnel flow conditions with $\mathrm{Re}=0.7-0.9\times10^6$ and a turbulence level of $Tu\leqslant1$ percent. Differences are observed only for the total pressure loss coefficients, where the experimental data are slightly higher than the numerical ones.

Because off-design performance and stall margin were two of the essential design goals during the optimization process, the experimental determination of the achievable flow angle range was of special interest. In particular, this validation was important because the optimization process provided profiles, which allow working ranges that are roughly 30 percent wider than ''conventional'' controlled diffusion blades designed for the same task. Such a theoretical comparison to a set of existing CDA profiles, using the four test cascades, is shown in Fig. 11 of the first part of this paper [1]. Happily, the present experiments using the four optimized test cascades confirmed each of the precalculated working ranges. Figure 9 provides the measured total pressure loss versus the incidence angle for cascade *A*, *B*, *C*, and *D*. For each cascade, the experimental working range $\Delta\beta_1$ is indicated and the corresponding design value is given in brackets. The working range hereby is defined in the conventional manner with $\Delta\beta_1=\beta_{1\max}-\beta_{1\min}$, with $\beta_{1\min}$ and $\beta_{1\max}$ as the flow angles where the losses achieve twice of the design point losses ($\omega=2\times\omega_D$).

Even cascade *D*, with a design working range of 27 deg achieved an experimental range of nearly 25 deg. Also the possible flow angle increase until stall onset, $\Delta\beta_{\mathrm{Stall}}$ at positive incidence, could be confirmed. Again, $\beta_{1\mathrm{Stall}}$ is achieved, when the losses become twice of the design point losses.

In addition to the experimental losses, Fig. 9 provides a comparison to theoretical losses from MISES with the Reynolds numbers and the turbulence level of the wind tunnel tests.

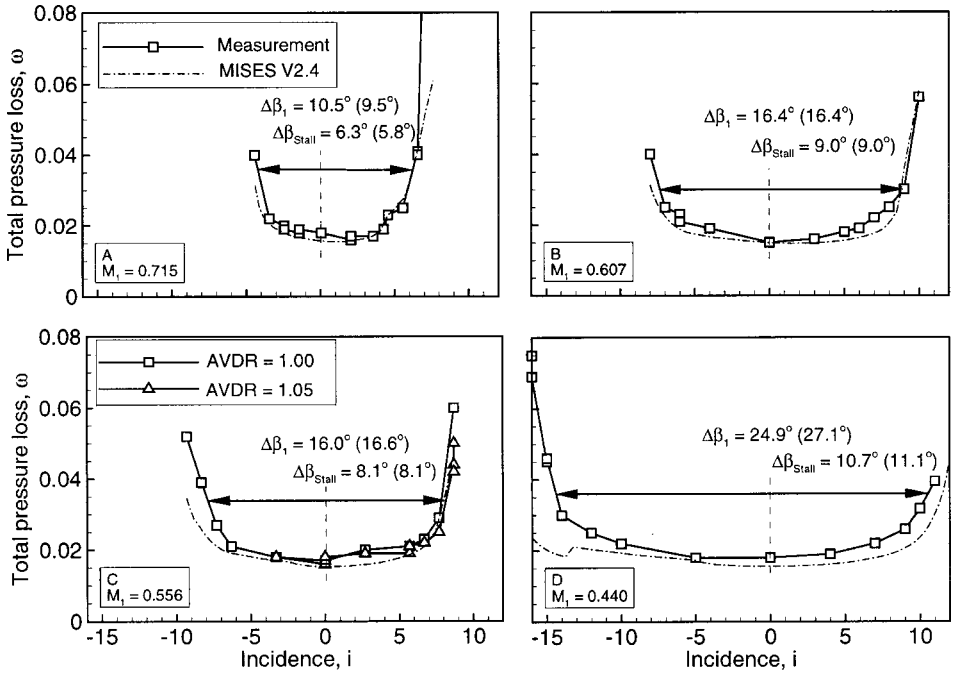

Fig. 9 Loss over incidence at design Mach number, experimental and MISES data, Re $=0.9-0.7\times10^6$, $Tu\leqslant1$ percent, experimental and design (in brackets) flow angle range

Table 4 Experimental and MISES data of test cascade *D* at $\mathrm{Re}=0.7\times10^6$ and $Tu=1.0$ percent

Incidence	-16°		0°		+9°		+11°	
	Experiment	MISES	Experiment	MISES	Experiment	MISES	Experiment	MISES
M_1	0.439	0.440	0.440	0.440	0.443	0.440	0.445	0.440
β_1	121.0°	121.0°	137.0°	137.0°	146.0°	146.0°	148.0°	148.0°
β_2	119.5°	118.2°	119.8°	119.3°	123.9°	121.9°	126.3°	124.4°
AVDR	0.99	0.99	1.00	0.99	1.00	0.99	0.99	0.99
ω	0.0695	0.0238	0.0179	0.0156	0.0262	0.0207	0.0395	0.0303

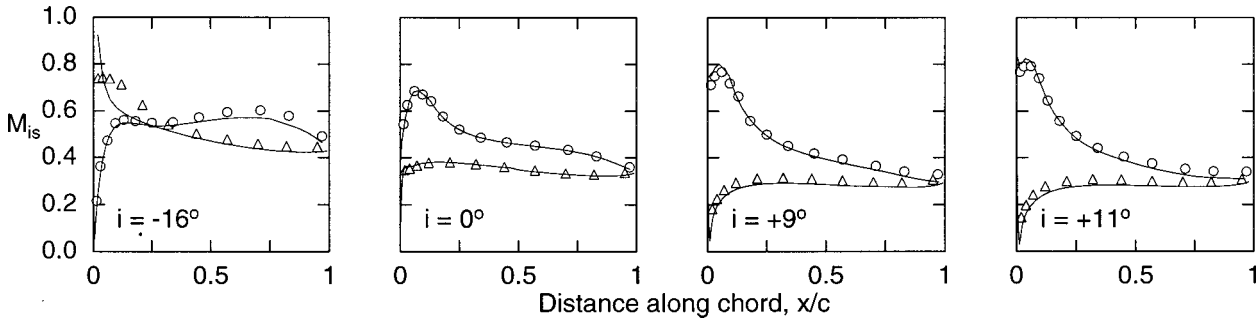

Fig. 10 Experimental and numerical Mach number distributions of test cascade *D*

Furthermore, representative for all cascades, Fig. 11 shows the dependency of the static pressure ratio and the exit flow angle on the inlet flow direction for both experiment and theoretical analysis. Noticeable is a gradual increase of the exit flow angle with positive incidences and a considerable deviation between experimental and theoretical values of up to 2 deg. This deviation, however, becomes less for very high incidences, when a strong boundary layer separation is simulated by the MISES code.

Profile Mach number distributions at off-design are discussed for cascade *D*, which has a wide incidence range of 25 degs, in Fig. 10 and the corresponding boundary conditions of the experiments and the simulation are provided in Table 4. Overall, the agreement to the MISES simulation was observed to be excellent in the entire working range. Only at an extreme negative incidence angle of -16 deg did MISES fail to calculate a severe separation at the pressure side leading edge. That also explains the relatively large discrepancy between measured and predicted losses in Fig. 9(*D*). At positive incidences, the small differences result from thicker experimental suction surface boundary layers and an increasing flow angle deviation. Overall, the off-design Mach number distributions shown in Fig. 10 are also representative for the other test cascades.

Navier–Stokes Analysis

It was of interest to know whether a Navier–Stokes solver would lead to even better agreement between experiment and simulation at positive incidences, where differences to the experimental exit flow angle (Fig. 11, top) were observed. Also, Navier–Stokes results can serve as an additional independent validation for the flow solver MISES applied during the design process.

Using cascade *B*, Navier–Stokes analyses have been performed on a computational domain extending from $-0.5c \leq x_{ax} \leq 1.9c$, where $x_{ax}=0$ corresponds to the blade leading edge. A multiblock grid with one *O*-block around the blade and four *I*-blocks was used with a total of 14,995 nodes. First grid spacing normal to the blade surface was chosen that yielded y^+ values between 2.0 and 3.0 within the boundary layer. The region near the leading edge has greater values, caused by the very thin boundary layer in this region. The DLR TRACE-U code [12,13], which has been developed to investigate steady and unsteady flow phenomena in turbomachines, has been used to perform the calculations. It allows multiblock grids and it is possible to perform two- or three-dimensional, steady or unsteady multistage calculations. Within the code, various numerical methods are implemented and can easily be exchanged. The essential ones used for the present Q3D steady-state calculations are as follows: The two-dimensional Reynolds-averaged Navier–Stokes equations are solved for a compressible ideal gas in conjunction with an eddy viscosity model. Convective fluxes are discretized using a second-order Roe-upwind TVD scheme and the viscous fluxes are discretized using central differences. The turbulence model used for the calculations is the one-equation approach developed by Spalart and Allmaras [14] and modified by Eulitz [13].

The simulation was performed with laminar/turbulent boundary layers on both suction and pressure sides and start of transition was taken from the MISES calculations. Inlet and exit boundaries

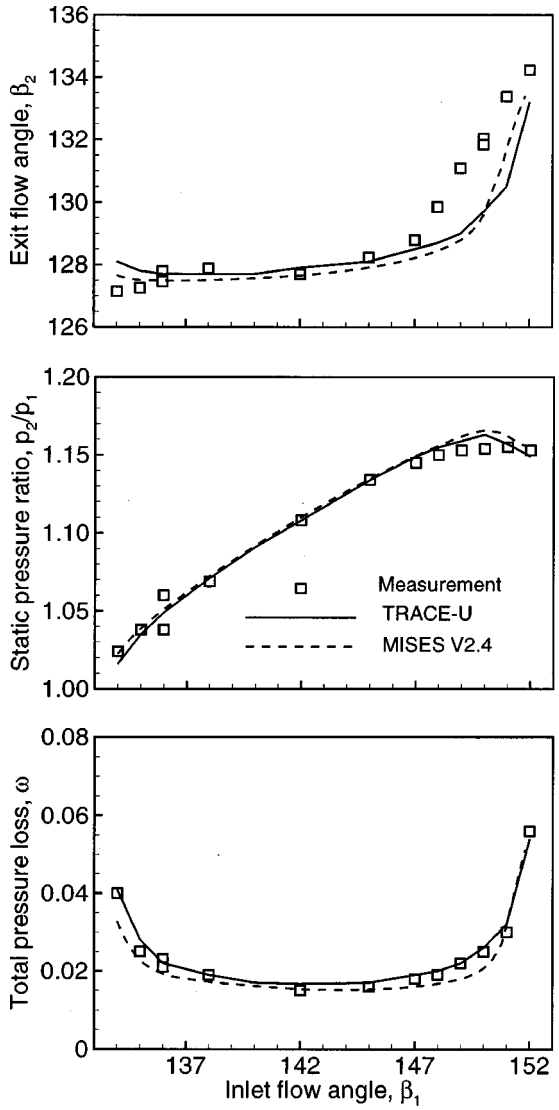

Fig. 11 Experimental performance data compared to MISES and Navier–Stokes calculations, cascade *B*, $M_1=0.607$, AVDR $=1.05$

are treated by nonreflecting boundary conditions according to Giles [15]. To simulate an axial stream tube variation, a linear stream tube thickness distribution from leading edge to trailing edge plane has been assumed. Spatial discretization is combined with a modified four-stage Runge–Kutta time stepping scheme. Implicit residual smoothing and local time stepping are used to accelerate convergence. The code has proven its reliability and high accuracy in cascade simulation even for highly loaded transonic flows [16].

Navier–Stokes calculations have been performed for the entire incidence range at the design Mach number of 0.607. The total pressure loss, static pressure ratio, and exit flow angle in Fig. 11 show good agreement between Navier–Stokes solution and experiment. Only the increasing exit flow angle at positive incidences could not be simulated accurately, although deviation to the experiments is something less in relation to MISES.

Even though the Navier–Stokes solver shows better agreement with all experimental data than MISES does, the differences from the MISES results are too marginal to justify its use in a design optimization process with extensive operating point calculations, due to an enormous increase in CPU time. On the other hand, it is a useful tool for validation after the design process and provides more information of critical flow conditions in addition to experimental investigations.

Boundary Layer Separation Behavior

Besides a wide inlet flow angle range, onset of boundary layer separation inside the blade rows is of specific interest for operation of a multistage compressor. The blade design optimization process, described in Part I of this paper, particularly asked for a wide margin between inlet flow angle at design and near stall ($\Delta\beta_{\mathrm{Stall}}$). The final optimized blade and cascade geometries of the new profile family fortunately showed this wide incidence range

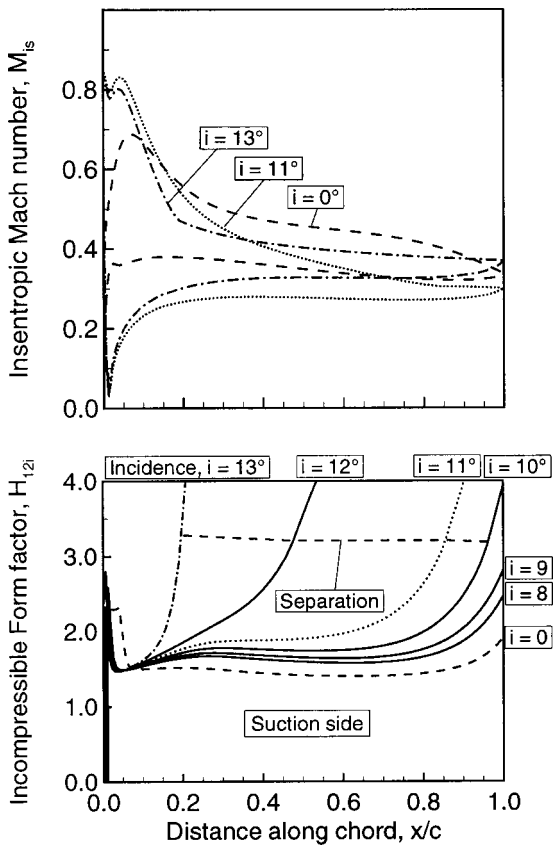

Fig. 12 Numerical separation behavior of cascade *D*, including MISES separation onset

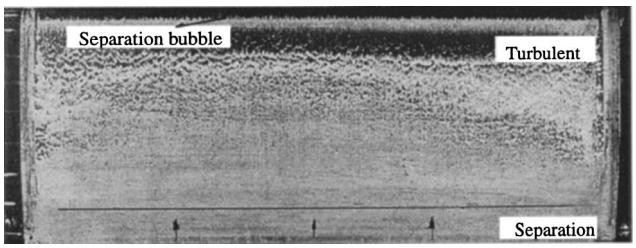

Fig. 13 Oil streak lines on the suction side of cascade *D*, $i=+9$ deg, flow direction from top to bottom

and especially a mild separation behavior. To discuss this behavior, profile Mach number distributions and the development of the suction surface form factor H_{12i} for design and high positive incidence angles are shown in Fig. 12. The distributions are calculated for cascade *D*, which showed a stall margin of about 11 deg. Qualitatively, these results are also typical for the other test cascades. At design ($i=0$, $\beta_1=137$ deg) the form factor remains constant from transition location to about 85 percent of chord. Farther downstream, however, a slight increase of the form factor is calculated, caused by an increase of suction surface curvature and a resulting further deceleration in the rear part. Increasing the incidence angle, the shape of this form factor distribution remains; however, the steep increase of H_{12i} successively moves forward, until H_{12i} exceeds a value of 2.5 to 2.8, that is commonly used as a criterion for separation onset. The horizontal dashed line in the lower part of Fig. 12 indicates separation ($c_f=0$) calculated with MISES. It corresponds to $H_{12i}=3.0+400./\mathrm{Re}_{\delta 2}$, implemented in MISES as the value for a change in boundary layer behavior.

Because the steep rise in H_{12i} is more or less concentrated on the rear part of the profile, boundary layer separation also remains concentrated on this rear blade portion. During a gradual rise in incidence from 8, 9, 10 to 11 deg, the separation line on the profile very slowly moves forward, but remains downstream of 85 percent of chord. Due to this, separation onset is very weak and no remarkable unsteady effects were observed in the experiment.

Surface flow visualization tests confirmed this observation. At an incidence angle of +9 deg (see Fig. 10) only little separation could be seen on the suction side of cascade *D*. The oil streak lines in Fig. 13 additionally visualize a small laminar separation bubble behind the velocity peak near the leading edge. Furthermore, nearly no secondary flow is observed on the blade surface, although blade loading with $i=+9$ deg is relatively high. This underlines the effectiveness of the end-wall boundary layer suction system.

Transition at High Reynolds Number

All calculations, using the modified Abu-Ghannam/Shaw criterion [5] with a high Reynolds number and turbulence level of 3 percent, showed transition within the accelerated front portion of the blade (see also results in Fig. 15, Part I of this paper). Therefore, the new high Reynolds number optimized profiles showed the characteristic front-loaded Mach number distribution. To ensure the design, it is of immense interest whether the transition location is predicted correctly or not. Most available experiments, either from stationary cascades or from real turbomachine blade rows, show that laminar flow is dominant on the accelerated part of the blade surface, even after a wake has passed the blade surface [17]. All these tests, however, have low Reynolds numbers ($\mathrm{Re}\leqslant 0.8\times 10^6$). There are not many data on transition location for the specific conditions, existing in large-scale heavy-duty gas turbines, such as high Reynolds numbers and high turbulence levels. One can find high Reynolds number tests for airplanes at low turbulence levels where boundary layers still remain laminar in an accelerated flow. There is a lack of data especially for favorable

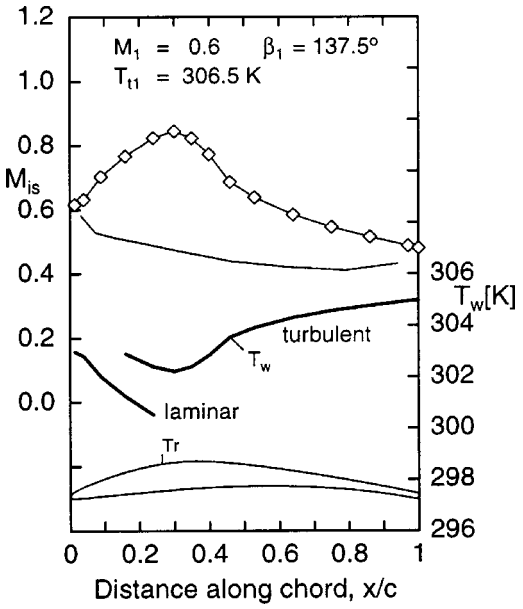

Fig. 14 Calculated adiabatic wall temperature on suction side and corresponding isentropic Mach number distribution

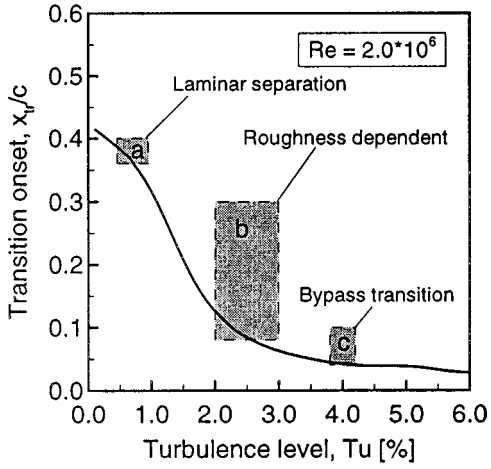

Fig. 16 Experimental (shaded area) and calculated (solid line) suction side transition onset for the profile shown in Fig. 14

pressure gradients, high Reynolds numbers, and higher turbulence levels, so an additional experiment has been performed to ensure the existence of early transition onset. A test cascade, shown in Fig. 14, was chosen, with an inlet Mach number of 0.6 and a suction side acceleration up to 35 percent of chord. Tests were run with Reynolds numbers from 0.7 to 2.7×10^6 and turbulence levels from about 0.7 to 4 percent. Liquid crystal coatings were used to detect transition by visualizing the difference in adiabatic wall temperature between laminar and turbulent flow which is in the order of 1–2 K for this experiment. A more detailed description of this technique is given by Steinert and Starken [18].

In Fig. 14 the adiabatic wall temperatures of the laminar and turbulent boundary layers are shown. The differences in temperature of the laminar and turbulent boundary layer is quite small (1–2 K), which made it necessary to have a very sensitive mixture of liquid crystals.

At usual wind tunnel test conditions without a turbulence screen and a low Reynolds number of about 0.8×10^6, suction surface flow along the front portion is laminar and a strong laminar separation bubble develops with transition near 40 percent of chord. Increasing the Reynolds number to 2.0×10^6, laminar flow in the front remains. Although the laminar separation bubble becomes less intensive, transition still occurs inside of the bubble (Fig. 15, left).

Increasing the turbulence level to a value of about 3 percent, the separation bubble disappears and a line of fully turbulent boundary layer moves forward to about 30 percent. When raising the turbulence level at this high Reynolds number, the sensitivity of the boundary layer to surface roughness increases considerably [19,20], as can be seen in the center of Fig. 15. More turbulence wedges become visible downstream of distinct roughness particles.

At about 4 percent turbulence intensity, obviously the bypass mechanism becomes dominant, and transition moves forward and is observed upstream of 10 percent of chord along the entire blade (Fig. 15, right).

A comparison of the visualized transition location to the predicted onset using the criterion implemented in MISES [5] is shown in Fig. 16. Overall, the forward movement of transition onset with a rising turbulence level is, at least qualitatively, well predicted. Some uncertainty remains between $Tu=2-4$ percent where surface roughness seems to have an additional influence.

Conclusions

A series of new compressor airfoils has been developed for high Reynolds number subsonic axial flow compressor stages in heavy-duty gas turbines by making use of a modern optimization technique. The design objective was a wide low-loss operating range and a specific stall margin. The new profiles, which have been optimized for high Reynolds numbers, showed relatively thick leading edges and a front loaded pressure distribution. The present experimental and theoretical analysis has demonstrated

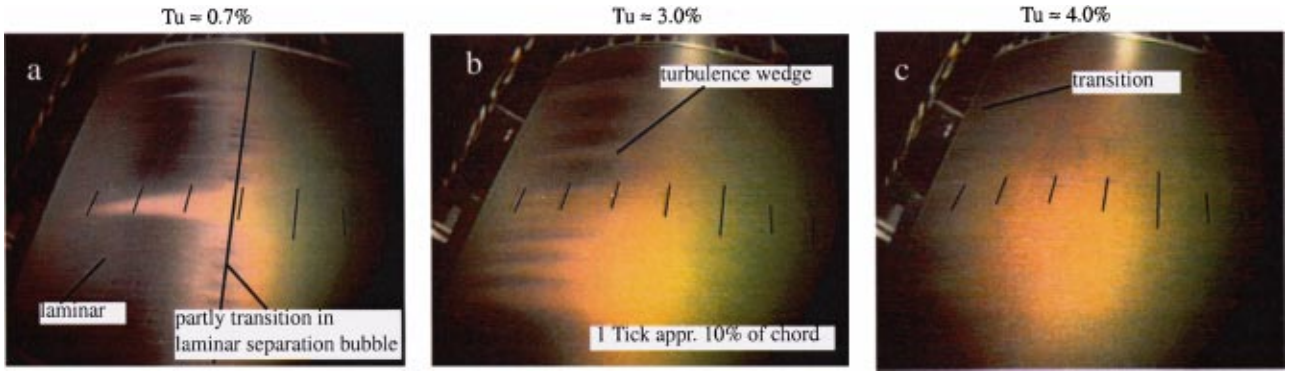

Fig. 15 Suction side transition visualized by liquid crystals, influence of turbulence level at $Re=2\times10^6$

the ability of the design tool and the superior aerodynamic performance of the profiles developed. Besides a practically exact verification of the precalculated design point conditions, the design flow angle range and stall margin could be confirmed. To ensure the design philosophy, which is based on early boundary layer transition on the blade surface, an additional basic experiment was performed that enlightened the effect of the turbulence level at high Reynolds numbers and favorable pressure gradient on transition onset. The experimental results at least qualitatively confirmed the transition model used.

Additional analyses of the complete operating range from negative to positive stall using a sophisticated Navier–Stokes flow solver did show somewhat better agreement with the experiment, but an essential advantage in relation to the inviscid/viscous interaction method used for this subsonic cascade flow could not be proved. The designers, however, are curious to know whether a complex method that simulates the real unsteady flow effects in a turbomachinery environment could alter the design profile pressure distribution, which has been optimized under steady flow conditions.

Nomenclature

AVDR = axial velocity density ratio $=(\rho_2 w_2 \sin\beta_2)/(\rho_1 w_1 \sin\beta_1)$
DF = diffusion factor $=1-w_2/w_1+(w_2/w_1\cos\beta_2-\cos\beta_1)s/2c$
H_{12i} = incompressible boundary layer form factor $=\delta_{1i}/\delta_{2i}$
M = Mach number
Re = Reynolds number $=w_1 c/\nu_1$
T = temperature
Tu = turbulence level
c = profile chord length
i = incidence angle $=\beta_1-\beta_{1\text{Design}}$
p = pressure
s = blade spacing, pitch
t = maximum profile thickness
w = velocity
x = coordinate in chordwise direction
x_{ax} = coordinate in axial direction
$\Delta\beta$ = flow turning $=\beta_1-\beta_2$
$\Delta\beta_1$ = incidence range from negative to positive stall
$\Delta\beta_{\text{Stall}}$ = incidence range from design to positive stall
β = flow angle with respect to cascade front
δ_1 = boundary layer displacement thickness
δ_2 = boundary layer momentum thickness
ν = kinematic viscosity
ρ = density
ω = total pressure loss coefficient $=(p_{t1}-p_{t2})/(p_{t1}-p_1)$

Subscripts

1 = inlet plane
2 = exit plane
is = isentropic entity
t = total, stagnation value
w = wall value

References

[1] Köller, U., Mönig, R., Küsters, B., and Schreiber, H. A., 2000, ''Development of Advanced Compressor Airfoils for Heavy-Duty Gas Turbines—Part I: Design and Optimization,'' ASME J. Turbomach., **122**, this issue, pp. 397–405.
[2] Drela, M., and Youngren, H., 1991, ''Viscous/Inviscid Method for Preliminary Design of Transonic Cascades,'' AIAA Paper No. 91-2364.
[3] Youngren, H., 1991, ''Analysis and Design of Transonic Cascades With Splitter Vanes,'' GTL Report No. 203, Mar., Cambridge, MA.
[4] Drela, M., and Youngren, H. 1996, ''A User's Guide to MISES 2.4,'' MIT Computational Aerospace Science Laboratory.
[5] Drela, M., 1995, ''Implementation of Modified Abu-Ghannam Shaw Transition Criterion,'' MISES User's Guide, MIT, Cambridge, MA.
[6] Abu-Ghannam, B. J., and Shaw, R., 1980, ''Natural transition of boundary layers—The effects of turbulence, pressure gradient and flow history,'' Journal of Mechanical Engineering Science, **22**, No. 5, pp. 213–228.
[7] Schulenberg, Th., Zimmermann, H., 1995, ''New Blade Design of Siemens Gas Turbines,'' presented at POWER-GEN Europe, May 16–18, Amsterdam.
[8] Köller, U., 1999, ''Entwicklung einer fortschrittlichen Profilsystematik für stationäre Gasturbinenverdichter,'' Dissertation, Ruhr Universität Bochum, Germany.
[9] Mayle, E., 1991, ''The Role of Laminar–Turbulent Transition in Gas Turbine Engines,'' ASME J. Turbomach., **113**, pp. 509–537.
[10] Schreiber, H. A., Starken, H., and Steinert, W., 1993, ''Transonic and Supersonic Cascades,'' AGARDOgraph ''Advanced Methods for Cascade Testing,'' Ch. Hirsch, ed., AGARD AG 328, pp. 35–59.
[11] Steinert, W., Fuchs, R., and Starken, H., 1992, ''Inlet Flow Angle Determination of Transonic Compressor Cascades,'' ASME J. Turbomach., **114**, No. 3, pp. 487–493.
[12] Eulitz, F., Engel, K., Pokorny, S., 1996, ''Numerical Investigation of Inviscid and Viscous Interaction in a Transonic Compressor,'' *Loss Mechanisms and Unsteady Flows in Turbomachines*, AGARD-CP-571, Paper No. 38.
[13] Eulitz, F., Engel, K., Gebing, H., 1996. ''Application of a one-equation eddy-viscosity model to unsteady turbomachinery flow,'' Engineering Turbulence Modeling and Experiments 3, W. Rodi and G. Bergeles, eds., Elsevier Science B.V. Amsterdam, pp. 741–751.
[14] Spalart, P. R., and Allmaras, S. R., 1992, ''A One-Equation Turbulence Model for Aerodynamic Flows,'' Paper No. AIAA-92-0439.
[15] Giles M. B., 1990, ''UNSFLO: A Numerical Method for the Calculation of the Unsteady Flow in Turbomachinery,'' GTL Rept. 205, Gas Turbine Laboratory, MIT, Cambridge, MA.
[16] Küsters, B., and Schreiber, H. A., 1998, ''Compressor Cascade Flow With Strong Shock-Wave/Boundary-Layer Interaction,'' AIAA J., **36**, No. 11, pp. 2072–2078.
[17] Halstead, D. E., Wisler, D. C., Okiishi, T. H., Walker, G. J., Hodson, H. P., and Shin, H. W., 1997, ''Boundary Layer Development in Axial Compressors and Turbines, Part 1–4,'' ASME J. Turbomach., **119**, pp. 114–127; 426–444; 225–237; 128–139.
[18] Steinert, W., and Starken, H., 1996, ''Off-Design Transition and Separation Behavior of a CDA Cascade,'' ASME J. Turbomach., **118**, pp. 204–210.
[19] Koch, C. C., and Smith, L. H., 1976, ''Loss Sources and Magnitudes in Axial-Flow Compressors,'' ASME J. Eng. Gas Turbines Power, **98**, pp. 411–424.
[20] Schäffler, A., 1980, ''Experimental and Analytical Investigation of the Effects of Reynolds Number and Blade Surface Roughness on Multistage Axial Flow Compressors,'' ASME J. Eng. Power, **102**, pp. 5–12.

Discussion: ''Development of Advanced Compressor Airfoils for Heavy-Duty Gas Turbines—Part II: Experimental and Theoretical Analysis'' [ASME J. Turbomach., 122, No. 3, pp. 406–414 (2000)][1]

N. A. Cumpsty
Whittle Laboratory, Cambridge University, Madingley Road, Cambridge, CB3 0DY, United Kingdom

My first aim in writing this discussion is to compliment the authors on two excellent papers. I found the results most interesting and the description and approach were a pleasure to read. The experimental confirmation was as near perfect as one has reason to hope for; as well as complimenting the authors my remarks also draw attention to the quality of the MISES code.

I have to admit that I had been skeptical of the benefits of automated optimization procedures. The results shown here, however, have arrived at a philosophy for optimum aerodynamic pressure distribution around the blades for very high Reynolds number, high free-stream turbulence, and modest inlet Mach number, which I would not have thought of. Because the explanation for the desirable features of the new blades is so clear, the successful solution seems in retrospect almost obvious; it clearly was not obvious and the authors are to be congratulated on their method

[1] Küsters, Bernhard, 2000, ''Development of Advanced Compressor Airfoils for Heavy-Duty Gas Turbines—Part II: Experimental and Theoretical Analysis,'' ASME Journal of Turbomachinery, Vol. 122, No. 3, pp. 406–414.

and their presentation. I am sure that this work will influence the blade profile shapes used in the future throughout the industry.

Figure 15 in the second paper, showing the surface flow visualization, is less clear than the pictures shown at the presentation in Indianapolis, which is a pity. What struck me at the conference is transition behavior which I had not seen before. As the turbulence level is raised at constant Reynolds number, the transition moves forward, but there is an intermediate range, around 3 percent free-stream turbulence, where the boundary layer turbulence starts near the leading edge as isolated wedges, presumably originating with small excrescences on the surface. In other words, the excrescences alone are not able to produce turbulence in the boundary layer because the local boundary layer Reynolds numbers is too low, but the interaction of free-stream turbulence of sufficient strength with the shear layer disturbance from these excrescences is able to initiate turbulence in the boundary layer.

Would the authors care to explain why their experiments were carried out at Reynolds numbers of about 10^6 and turbulence of about 1 percent, whereas the designs were at much higher values of both parameters? Surely the thrust of the design was that a different transition behavior is expected when the Reynolds number is higher than is common in aircraft engines and high free-stream turbulence is allowed for. (There is no reason to expect the turbulence levels to be significantly different for large land-based engines or aircraft engines.) If transition is going to occur in the region of flow acceleration on the suction surface, there is no benefit in having the peak suction well back on the chord. The optimum shape for the blades should therefore be different for the conditions of the design and the conditions of the tests. Given that the tests were carried out at Reynolds numbers much lower than design, in the range more typical of aircraft engines, and with relatively low free-stream turbulence, what does the agreement of measurements with calculations at high Reynolds number and turbulence intensity tell us? Does it say that at the comparatively low inlet Mach numbers used for these blades the exact nature of the blade shape and pressure distribution is not very important? Going back to NASA SP-36, Fig. 130 shows how loss is relatively insensitive to blade profile shape for inlet Mach numbers below about 0.8.

Closure to ''Discussion of 'Development of Advanced Compressor Airfoils for Heavy-Duty Gas Turbines—Part II: Experimental and Theoretical Analysis''' [ASME J. Turbomach., 122, No. 3, pp. 406–414 (2000)]

We would like to thank Professor Cumpsty for the encouraging and interesting comments on our contribution. During the course of the work we also have been pleased to see that by applying the automated design tool, the blade profiles and the blade pressure distribution followed the prescribed boundary conditions and the constraints that have been formulated in the objective function. Among other things, it became clear how the blade pressure distribution on the suction side reacts on boundary layer transition location and that early transition encourages a forward movement of the suction side maximum velocity.

He clearly recognized from our visualization experiment, which is presented in the second part of the paper, that boundary layer transition onset likewise depends on the free-stream turbulence level and surface roughness. This phenomenon has not been studied in detail so far, but we are aware that both the disturbances downstream of single roughness particles on the shear layer and the disturbances due to free-stream turbulence seem to interact in a complex mechanism. The clarification of this phenomenon, however, has not been the objective of the present paper. At this time, first of all, we wanted to supply evidence on upstream propagation of transition onset into the accelerated front portion of the blade with increasing free-stream turbulence *and* increasing Reynolds number. Further results and information on this Reynolds number and turbulence influence are discussed in an additional paper [1].

The extensive experiments to validate the new profile design and especially the MISES code employed were carried out at Reynolds numbers around 0.8×10^6 for two reasons: First, to limit energy consumption and blade loading, the total pressure was kept around 1.1 bar; second, short blade chord with an acceptable blade aspect ratio of 2.4 helped to limit endwall and secondary flow effects. Furthermore, no turbulence grids have been installed upstream of the test section, to ensure an undisturbed flow field with homogeneous inlet flow that allows highest measurement accuracy and periodicity.

The cascade performance results presented in the paper, from both experiment and simulation, show good agreement, although the tests had been performed at low Reynolds numbers and a low turbulence level and the design calculations were carried out at turbomachinery conditions when Reynolds number and turbulence level are high. The good agreement between measured low-Reynolds-number data and the calculated loss and flow turning values for higher Reynolds numbers and free-stream turbulence levels is based on the low shift in suction side transition location for these specific front-loaded profiles. While the calculated values show the suction side transition in the first 10 percent of chord, under the test conditions the velocity distributions of the airfoils encourage transition to occur a short distance after the suction side maximum, which is close to 10 percent of the chord length. Hence, in both cases, the suction side boundary layer, especially in the region of strong adverse pressure gradients, behaves similarly. This coincidence is responsible for the good accordance between test and calculation.

The answer to the last question is no. If one really looks in detail, it has been shown over the years that for subsonic Mach numbers up to 0.7 or 0.8, the total pressure loss level in the vicinity of the design point is not essentially dependent on the blade profile shape; presumably the data are compared for the same velocity triangles and cascade solidities. But for higher aerodynamic blade loading, and especially at off-design conditions, large differences are observed because the boundary layer behavior and resulting losses really depend on the blade and cascade geometry. Not solely optimizing at design point conditions, but reaching excellent off-design performance with large stall margin, is the advantage of the new design approach.

References

[1] Schreiber, H. A., Steinert, W., and Küsters, B., 2000, ''Effects of Reynolds Number and Free-Stream Turbulence on Boundary Layer Transition in a Compressor Cascade,'' ASME Paper No. 2000-GT-263.

